Nanoscale

PAPER

View Article Online
View Journal | View Issue

Cite this: *Nanoscale*, 2016, **8**, 15658

Engineering the hot spots in squared arrays of gold nanoparticles on a silver film

Anran Li,[a] Sachin K. Srivastava,[a] Ibrahim Abdulhalim*[a,b] and Shuzhou Li*[a]

Density of nanoparticle (NP) arrays affects the hot spots distribution and strength in NP-metal film (NP-MF) geometry. In-depth understanding of the variation of electromagnetic (EM) field enhancement with NPs density is essential for wide applications of the NP-MF geometry such as surface-enhanced spectroscopies and enhanced efficiency of optoelectronic devices. Here, we show that the field distribution in the NP array on the metal film is greatly enhanced and confined at the NP–NP junctions for very small horizontal gap (*g*) between neighboring NPs, whereas the fields at the NP-MF junction are extremely small. When gradually increasing *g*, the field enhancement at the NP–NP junction decreases, along with the gradually enhanced fields at the NP-MF junction. We show that there is an optimal value of horizontal gap (~75 nm for 80 nm Au NP array on Ag film with 532 nm normal incidence), indicating that the average field enhancement in NP-MF geometry can be optimized by adjusting the horizontal gap. More importantly, it is found that the EM field enhancement is greatly decreased when *g* fulfills the requirement to couple the 532 nm incident light into SPPs, because of the interference between the LSPR and the SPPs, which leads to a Fano dip at the incident wavelength of 532 nm.

Received 7th May 2016,
Accepted 27th July 2016

DOI: 10.1039/c6nr03692a

www.rsc.org/nanoscale

Introduction

Noble metal nanoparticles (NPs) have attracted considerable interest in the fields of surface-enhanced spectroscopies, refractive index sensing, photo-thermal therapy and imaging, photocatalysis, and water splitting because of their ability to generate huge electromagnetic (EM) field enhancement arising from the localized surface plasmon resonances (LSPRs).[1–6] LSPR is the coherent oscillation of free electrons at the NP surface.[1] Previous studies have shown that the LSPRs of NPs strongly depend on the NPs' composition, shape, and size.[7–9] In the past, the LSPRs of NPs with various geometries have been extensively explored such as nanospheres, nanorods, spiky structures, NP dimers, and NP-metal film (NP-MF).[10–14]

Among the abovementioned nanostructures, the metal NP on the metal film system has received increasing attention, for not only its convenient fabrication but also its ability to confine EM fields in the gap between the NP and the film.[15–20] The NP-MF geometry can be fabricated over large areas using low-cost and simple methods by directly depositing the NPs onto a metal-coated substrate.[16,18,21] Compared with NP assembly, the nanogaps in NP-MF geometry are more controllable, particularly for the sub-nanometer gap sizes.[18,19,21–26] In addition, the NP-MF provides intensely enhanced EM fields at the junction between the NP and the film, resulting from the coupling between the NP and its mirror image in the metal film.[18,22,27] Moreover, the EM fields in NP-MF geometry are confined at the surface of the metal film, making it much easier to insert the analytes or targets into regions with a huge EM field enhancement, particularly when the targets are 2D materials (for example, graphene and MoS_2).[26,28–32] Ascribing to the abovementioned advantages, NP-MF systems have been widely explored for applications in surface-enhanced spectroscopies (SES), photovoltaic devices, and light trapping.[32–36]

Wide applications of the NP-MF geometries depend on the comprehensive understanding of the EM field enhancement in them. In previous studies, huge efforts have been devoted to optimizing the hot spots in NP-MF configurations. It was shown that 80–100 nm Au NPs give the largest relative Raman signal per NP for the NP-MF system under study, when using a 632.8 nm He–Ne laser with 58° incidence angle.[37] Compared with the nanosphere-film, the nanostar-film could generate much higher EM field enhancement at the junction between the nanostar and the film, resulting in a much larger surface-enhanced Raman scattering enhancement factor.[38] The separation distance between the NP and the film also plays an important role on the EM field enhancement in NP-MF, wherein the average field enhancement over the NP surface gradually decreases with increasing gap sizes.[18] Researchers also found that NP dimers on the metal film can generate

[a]*School of Materials Science and Engineering, NTU-HUJ-BGU NEW CREATE Programme, Nanyang Technological University, 639798, Singapore. E-mail: lisz@ntu.edu.sg, Abdulhlm@bgu.ac.il*
[b]*Department of Electro-optic Engineering & Ilse Katz Institute for Nanoscale Sciences and Technology, Ben Gurion University of the Negev, Beer sheva-84105, Israel*

higher EM field enhancement in the dimer-film gap than the single NP on the film.[32,39,40] The effects of surface roughness and metal film thickness on the plasmonic properties of Au NPs on an Au film were also investigated.[39,41]

Compared with an isolated NP on the metal film, the periodic NP arrays on the metal film exhibit more fascinating properties, since the periodic array can provide additional momentum $G = (2\pi/p)\sqrt{i^2 + j^2}$ to couple the incident light into surface plasmon polaritons (SPPs) on the metal film.[20,42] Here, p is the periodicity of the NP array, and i and j are integers representing the Fourier harmonics of a periodic structure along x and y, respectively. Researchers have found that huge EM field enhancement can be obtained when the resonance peak of the SPP coincides with that of the LSPR.[43,44] In addition, the periodicity of the NP array determines hot spots density, since each NP-MF junction can serve as a hot spot. It has been shown that the hot spots density plays a significant role in SERS.[45] Therefore, it is important to know how the NP density affects the hot spot distribution and density in the metal NP array on the metal film configuration. In previous studies about the interference between the LSPR and the SPP, the periodicity of the NP array has been tuned to adjust the SPP resonance position.[42–44] Nevertheless, in these studies, the periodicity of the NP array was gradually increased by several hundred nanometers. The NP array with small periodicity has not been investigated wherein the coupling between adjacent NPs is strong.

In this article, taking the Au square NP array on the Ag film as an example, the effects of the NP density on the distribution and intensity of EM fields in the metallic NP array on the metal film are carefully examined by gradually increasing the horizontal gap (g) between neighboring NPs from 2 nm to 1100 nm. We show that the EM fields are greatly enhanced and confined at the NP–NP junctions for very small g, whereas the EM field enhancement at the NP-MF junction is rather small. With increasing g, the EM field enhancement at the NP–NP junction decreases, along with the gradually increased field enhancement at the NP-MF junction, until g is larger than one certain value, wherein the EM field enhancement only slightly varied with further increase in g. In addition, we find that the EM field enhancement will be drastically decreased when g fulfills the requirement to couple the 532 nm incident light into SPPs, because of the interference between the LSPR and the SPPs.

Numerical method

The optical properties of the square Au NP array on the Ag film are investigated using the 3D finite-difference time-domain (FDTD) method.[46] Fig. 1 shows the schematic of the square Au NP array on top of a thin Ag film. Since the thickness of a monolayer molecules is 1–2 nm, the separation between the Au NP and the Ag film is set at 2 nm. A 2 nm gap gives a large electric field enhancement, wherein quantum tunneling effects are negligible.[19,21] The diameter of the Au NP is set at

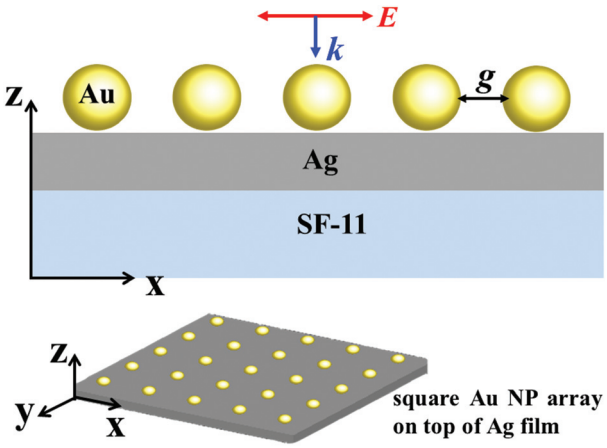

Fig. 1 Schematic of the square Au NP array on top of the Ag film. The polarization direction and wave vector of the incident light are denoted by $\vec{E}$ and $\vec{k}$, respectively.

80 nm, which has been shown to yield a larger SERS enhancement factor.[37] The thickness of the Ag film is 47 nm. g represents the horizontal gap between two adjacent Au NPs. In all simulations, a plane wave source polarized along x direction with 532 nm wavelength is incident normally from the top. In order to simulate the infinite Ag film and the Au NP array, periodic boundary conditions are used in all calculations. The dielectric constants of Au and Ag are obtained from Johnson and Christy,[47] and from Palik,[48] respectively. The refractive index of the substrate is set to 1.7948, which is the refractive index of SF-11 glass. Surrounding medium is vacuum. To obtain accurate results, override mesh region with 1 nm mesh size is used to cover the Au sphere and Ag film. Before all the simulations, convergence testing was carefully done to verify the accuracy and stability of the calculations. In this study, all the calculations are performed using the FDTD simulation program (FDTD solutions 8.6, Lumerical solutions, Inc., Vancouver, Canada).

Results and discussion

First, we try to find the NP array that can couple the 532 nm incident light into SPPs. The wave vector of SPPs excited on the metal-dielectric interface is

$$k_{sp} = k_0\sqrt{\frac{\varepsilon_m\varepsilon_d}{\varepsilon_m + \varepsilon_d}} \quad (1)$$

where $k_0 = \omega/c = 2\pi/\lambda$ is the free-space wave vector; ω is the frequency of the incident light, c is the velocity of light in vacuum, λ is the incident wavelength; ε_m and ε_d are the complex dielectric constants of the metal and the dielectric medium, respectively. Due to the momentum mismatch, SPPs on a smooth thin metallic film cannot be directly excited by free space incidence.[49] When a NP array is deposited on a metal film, the periodic array can provide additional momentum $G = (2\pi/p)\sqrt{i^2 + j^2}$. To couple the incident light into

SPPs, the periodicity of the NP array should fulfill the following condition:

$$(2\pi/p)\sqrt{i^2+j^2} = k_0\sqrt{\frac{\varepsilon_m\varepsilon_d}{\varepsilon_m+\varepsilon_d}} = (2\pi/\lambda)\sqrt{\frac{\varepsilon_m\varepsilon_d}{\varepsilon_m+\varepsilon_d}} \quad (2)$$

According to eqn (2), the periodicities required to couple the 532 nm incident light into SPPs are 505 nm, 714.5 nm, 931 nm, and 1130 nm, respectively, for (i, j) equals to (1, 0), (1, 1), (2, 0), and (2, 1). Therefore, in the following simulations, g is gradually changed from 2 nm to 1100 nm (equals p–d with d being the NP diameter), with four specific values being 425 nm, 634.5 nm, 931 nm, and 1050 nm (corresponding to the periodicity p of 505 nm, 714.5 nm, 1011 nm, and 1130 nm, respectively).

Effects of the horizontal gap on the EM field enhancement between the NPs and MF

For analytes or targets deposited on top of the Ag film, the field enhancement at the top surface of the Ag film plays a dominant role on their optical processes. Fig. 2 shows the effects of g on the maximum and the average field enhancement at the top surface of the Ag film. Here, the average field enhancement at the top surface of Ag film is obtained by averaging over the region within a layer of 2 nm thickness above the top surface of the Ag film (the spacer thickness, *i.e.*, the deposited analytes thickness). As shown in Fig. 2(a), the maximum EM field enhancement is extremely small when g is 2 nm. With gradually increasing g, the maximum enhancement increases and reaches its maximum value of 808 when g equals to 400 nm. In addition, the maximum field enhancement in Au NP array on the Ag film begins to exceed that in an isolated Au NP on the Ag film when g is larger than 200 nm. The maximum field enhancement in an isolated Au NP on the Ag film is shown by the dashed line in Fig. 2(a). With further increase of g from 400 nm to 1100 nm, the maximum field enhancement tends to be constant, except for the surprising sharp drops at g equals to 425 nm, 634.5 nm, 931 nm, and 1050 nm. At these values, the periodicity of the NP array is 505 nm, 714.5 nm, 1011 nm, and 1130 nm. According to eqn (2), these periodicities are exactly the ones that can provide additional momentum to couple the 532 nm incident light to SPPs. Fig. 2(b) shows the effects of g on the average field enhancement at the Ag film surface. The results show that the average EM field enhancement is very small when g is 2 nm. With increasing g from 2 nm to 75 nm, a rapid increase of the average field enhancement from 0.63 to 11 is observed. With further increasing g, the average EM enhancement shows a gradual decrease. The results indicate that the optimal g for the average field enhancement for 80 nm Au NPs on the Ag film at 532 nm normal incidence is ~75 nm. The origin of this optimum will be further discussed below.

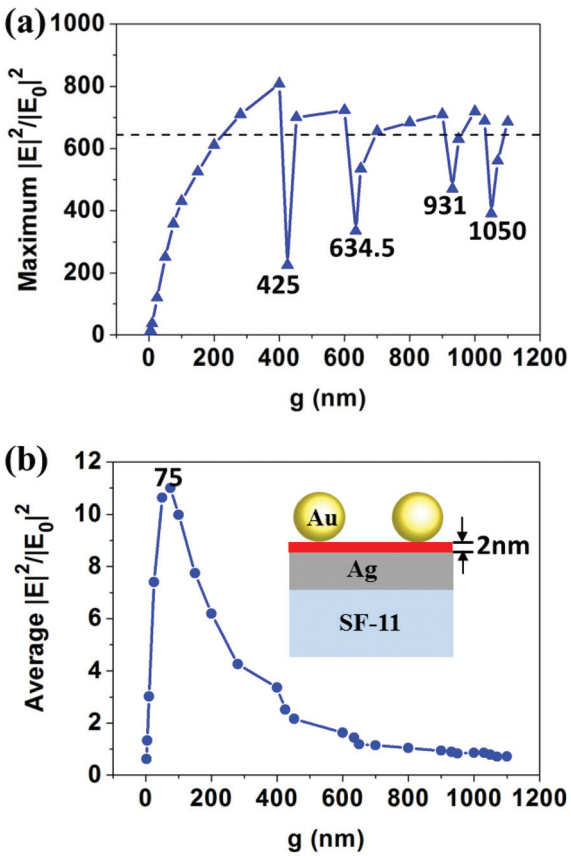

Fig. 2 Effects of the horizontal gap (g) between neighboring Au NPs on (a) the maximum, and (b) the average EM field enhancement at the top surface of the Ag film. The dashed black line in (a) shows the maximum EM field enhancement of an isolated Au NP on Ag film. The red color in the inset of (b) shows the region where the average field enhancement is calculated.

Effects of the horizontal gap on the EM field enhancement between the NPs

EM field enhancement at the surface of the NP is also very important, particularly when the analytes are decorated on the NPs. Hence, the effects of the horizontal gap g on the field enhancement at the surface of the Au NP are further investigated (Fig. 3). Here, the maximum field enhancement at the interparticle junction between neighboring Au NPs is monitored. The average field enhancement is calculated using the equation $\int |E|^2 ds / \int ds$, which averages the field enhancement over the spherical surface 1 nm away from the Au NP surface. In order to show the change of the maximum field enhancement more clearly, the EM field enhancement is plotted in the logarithmic scale. As shown in Fig. 3(a), the field enhancement at the junction between two Au NPs is as large as 1040 when g is 2 nm. With increasing g, the enhancement at the interparticle junction decreases rapidly. When g is larger than 10 nm, the maximum enhancement at the NP–NP junction becomes even smaller than the value for an isolated Au NP on the Ag film. When g is larger than 200 nm, the maximum enhancement in the Au NP array on the Ag film geometry is comparable with that in the single Au NP on the Ag film. In addition, four small down jumps of the maximum enhancement are observed at g equals to 425 nm, 634.5 nm, 931 nm, and 1050 nm as shown in Fig. 3(a). The change of the average field

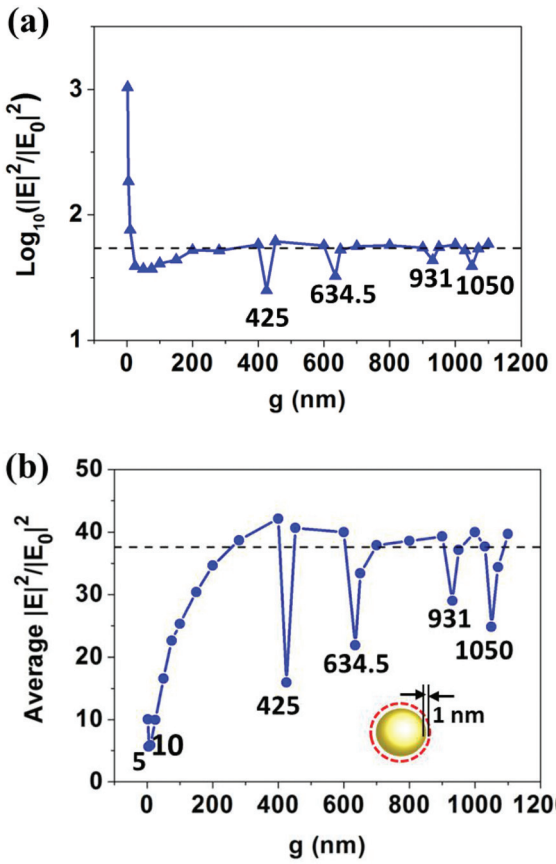

Fig. 3 Effects of the horizontal gap (g) between two adjacent Au NPs on (a) the maximum EM field enhancement at the interparticle junction between two adjacent Au NPs, and (b) the average EM field enhancement at the surface of the Au NP. The dashed black line in (a) and (b) shows the maximum and the average field enhancements for an isolated Au NP on the Ag film, respectively. The dashed red line in the inset of (b) shows the spherical surface 1 nm away from the NP surface where the average field enhancement is calculated.

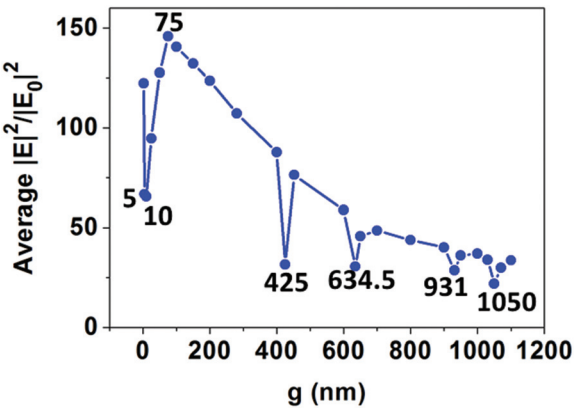

Fig. 4 Modified average EM field enhancement at the surface of the Au NP for various horizontal gaps (g) between two adjacent Au NPs by taking the NP density into account.

enhancement at the Au NP surface with g is shown in Fig. 3(b). At the very beginning, a decrease of the average field enhancement from 10 to 7 is observed when g is increased from 2 nm to 5 nm. With further increasing g, the average enhancement gradually increases and reaches the maximum value of 42.17 at g = 400 nm. When g = 300 nm, the average field enhancement over the NP surface becomes larger than that in the case of a single NP on the Ag film. When g is larger than 400 nm, continuous increase of g shows negligible effects on the average enhancement, except for g equals to 425 nm, 634.5 nm, 931 nm, and 1050 nm, wherein unusual sharp drops of the average field enhancement are again observed.

When the analytes are decorated on the Au NP surface, the entire signals from these analytes are determined by both the average electric field enhancement over a single NP surface and the number of the NPs within the spot size of the incident light. For NP arrays, the number of the NPs within the spot size of the incident light is determined by the periodicity of the array. If the spot size of the incident light is A, and the periodicity of the NP array is p, then the number of the NPs within the spot size is $A/(p \times p)$. The geometrical factor f is then defined as $A/(p \times p)$. By multiplying the data in Fig. 3(b) by f, the modified average electric field enhancement is obtained, which considers the effects of the number of NPs. Based on the modified average electric field enhancement, the optimal g for the overall signal enhancement can be obtained. Even though the value of the modified average field enhancement varies with different A, the optimal g for the average field enhancement does not change with A. Therefore, we can set A to one specific value to quantify the modified average field enhancement, and hence obtain the optimal g. The modified average field enhancement on the NP surface by assuming A of 1 μm^2 is shown in Fig. 4. The results indicate that when the NP density is considered, the optimal g for the average field enhancement over the NP surface is at ~75 nm.

Origin of the observed horizontal gap effects on the distribution and intensity of EM fields

In order to understand the change of the EM field enhancement with increasing g, the field distributions in the array NP-MF case with various g values are calculated (Fig. 5). The results indicate that when g is 2 nm, extremely enhanced EM fields are generated and confined at the junction between two Au NPs, which can be ascribed to the strong interparticle coupling between two Au NPs. However, when g is 2 nm, the field enhancement at the NP-MF junction is extremely small, which may be caused by the strong scattering and absorption of the incident light by the dense NPs.[44,50] With increasing g, the field enhancement at the horizontal gap between two Au NPs rapidly decreases because of the decreased interparticle coupling strength. At the same time, more regions over the NP surface become lightened up, which can be ascribed to the LSPR of a single Au NP. The increase of g also leads to the decreased scattering and absorption of the incident light by NPs. Therefore, the field enhancement at the NP-MF junction gradually increases with increasing g. Fig. 3(a) indicates that

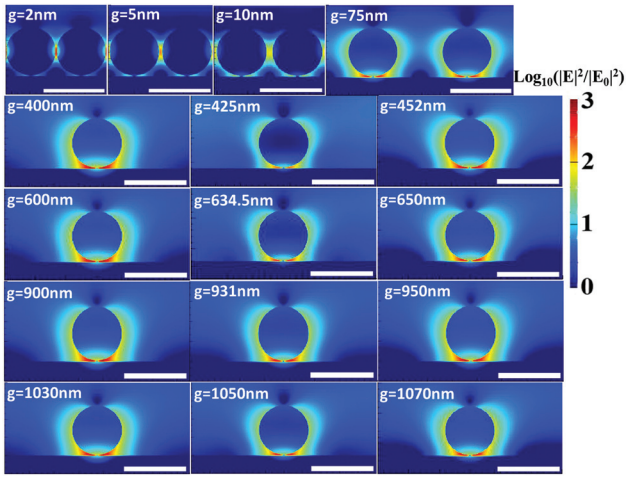

Fig. 5 EM field distributions ($\log_{10}(|E|^2/|E_0|^2)$) at *xz* plane of the Au NP array on Ag film with various *g* under normal incidence at 532 nm. The scale bar in each figure is 100 nm.

the maximum enhancement at the NP–NP junction is even smaller than that in a single Au NP on the Ag film geometry for *g* varying from 10 nm to 150 nm. This can be explained by both the decreased coupling strength between neighboring NPs and the difference between the LSPR wavelength and the incident wavelength caused by interparticle coupling. When *g* is large enough (>200 nm), the coupling between two Au NPs is negligible. In this case, further increasing *g* has negligible effects on the field distributions. As shown in Fig. 5, the field distributions for the NP-MF case is almost the same for the *g* values at 400 nm, 452 nm, 600 nm, 650 nm, 900 nm, 950 nm, 1030 nm, and 1070 nm. Therefore, when *g* is large enough, the maximum enhancements at both the top surface of the Ag film and the interparticle junction between two Au NPs show only slight variations with further increase in *g*.

Fig. 2 and 3 show that an unusual decrease of the EM field enhancement is generated at the *g* values of 425 nm, 634.5 nm, 931 nm, and 1050 nm. This can also be intuitively seen from the calculated EM field distributions in Fig. 5. Based on our calculations, Au NP arrays with these gaps are exactly the ones that can couple the 532 nm incident light into SPPs. The abrupt decrease of the field enhancement at these *g* values could be explained by the Fano resonance between the SPPs mode and the LSPR mode.[51] As shown in Fig. 6(a), two resonance peaks can be observed for the Au NP array on the Ag film with *g* at 425 nm, 634.5 nm, 931 nm, and 1050 nm. The resonance peak at the shorter wavelength can be ascribed to the SPPs mode, which is close to the wavelength of the SPPs calculated from eqn (1) (at ~505 nm with incident wavelength of 532 nm). Moreover, the resonance peak at the longer wavelength can be ascribed to the LSPR mode of the Au NP. It can also be noted that a small peak at ~590 nm is observed for g = 1050 nm, which corresponds to the $(i, j) = (2, 0)$ SPP mode coupled with the free-space wavelength of 590 nm. Fig. 6(a) shows that there are some shifts of the resonance peaks for different *g* values. Nevertheless, the resonance dips for *g* at

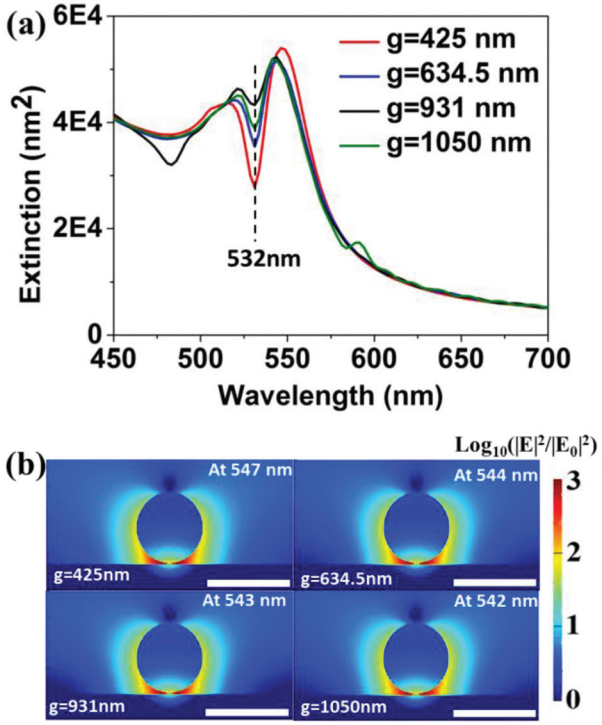

Fig. 6 (a) Calculated extinction cross sections of the Au NP array on the Ag film with *g* values at 425 nm, 634.5 nm, 931 nm, and 1050 nm. (b) EM field distributions ($\log_{10}(|E|^2/|E_0|^2)$) at *xz* plane of the Au NP array on an Ag film at various *g* values at their corresponding resonant wavelength. The scale bar in each figure is 100 nm.

425 nm, 634.5 nm, 931 nm, and 1050 nm are at ~532 nm. Therefore, the EM field enhancement is greatly decreased at 532 nm incident wavelength. The EM field distributions are also calculated for the Au NP array on the Ag film for various *g* values at their corresponding longer resonant wavelengths rather than at 532 nm. As shown in Fig. 6(b), greatly enhanced electric fields are generated in the Au NP array on the Ag film at their corresponding resonant wavelength.

Conclusions

In summary, it is shown that the horizontal gap (*g*) between neighboring NPs has a significant effect on the EM field enhancement in a square Au NP array on the Ag film. When *g* is very small (2 nm), the EM fields are greatly enhanced and confined at the NP–NP junctions because of the strong interparticle coupling between two NPs, whereas the field enhancement at the NP-MF junction is rather small because of the large scattering and absorption of the incident light by the dense NPs. With gradually increasing *g*, the enhancement at the NP-MF junction increases and the enhancement at the NP–NP junction decreases until they reach a relatively constant value. In addition, the results indicate that the average field enhancement in the array of NP-MF geometry can be optimized by changing *g* values. In this manuscript, for 80 nm

Au NP on the Ag film at incident wavelength of 532 nm, g at ~75 nm gives the largest average EM field enhancement at the Ag film surface and the Au NP surface. More importantly, the results indicate that the EM field enhancement is greatly decreased when g fulfills the requirement to couple the 532 nm incident light into SPPs. We show that the drastically decreased field enhancement is due to the Fano interference between the LSPR and the SPPs, which leads to a Fano dip at the incident wavelength of 532 nm. These results are very important for designing enhanced spectroscopy experiments and other applications of the NPs on metal film geometry.

Acknowledgements

This research is conducted by NTU-HUJ-BGU Nanomaterials for Energy and Water Management Programme under the Campus for Research Excellence and Technological Enterprise (CREATE), which is supported by the National Research Foundation, Prime Minister's Office, Singapore.

Notes and references

1 K. A. Willets and R. P. Van Duyne, *Annu. Rev. Phys. Chem.*, 2007, **58**, 267–297.
2 A. Li, S. Isaacs, I. Abdulhalim and S. Li, *J. Phys. Chem. C*, 2015, **119**, 19382–19389.
3 Y. Tang, Z. Jiang, G. Xing, A. Li, P. D. Kanhere, Y. Zhang, T. C. Sum, S. Li, X. Chen, Z. Dong and Z. Chen, *Adv. Funct. Mater.*, 2013, **23**, 2932–2940.
4 L. Zhang, Y. Zhang, Y. Hu, Q. Fan, W. Yang, A. Li, S. Li, W. Huang and L. Wang, *Chem. Commun.*, 2015, **51**, 294–297.
5 X. Ding, C. H. Liow, M. Zhang, R. Huang, C. Li, H. Shen, M. Liu, Y. Zou, N. Gao, Z. Zhang, Y. Li, Q. Wang, S. Li and J. Jiang, *J. Am. Chem. Soc.*, 2014, **136**, 15684–15693.
6 Z. Zhang, A. Li, S. W. Cao, M. Bosman, S. Li and C. Xue, *Nanoscale*, 2014, **6**, 5217–5222.
7 N. J. Halas, S. Lal, W. S. Chang, S. Link and P. Nordlander, *Chem. Rev.*, 2011, **111**, 3913–3961.
8 J. M. Romo-Herrera, R. A. Alvarez-Puebla and L. M. Liz-Marzán, *Nanoscale*, 2011, **3**, 1304–1315.
9 M. Rycenga, C. M. Cobley, J. Zeng, W. Li, C. H. Moran, Q. Zhang, D. Qin and Y. Xia, *Chem. Rev.*, 2011, **111**, 3669–3712.
10 A. Li and S. Li, *Nanoscale*, 2014, **6**, 12921–12928.
11 S. Kessentini, D. Barchiesi, C. D'Andrea, A. Toma, N. Guillot, E. Di Fabrizio, B. Fazio, O. M. Maragó, P. G. Gucciardi and M. Lamy de la Chapelle, *J. Phys. Chem. C*, 2014, **118**, 3209–3219.
12 S. Pedireddy, A. Li, M. Bosman, I. Y. Phang, S. Li and X. Y. Ling, *J. Phys. Chem. C*, 2013, **117**, 16640–16649.
13 H. Chen, L. Shao, Q. Li and J. Wang, *Chem. Soc. Rev.*, 2013, **42**, 2679–2724.
14 E. Ringe, B. Sharma, A.-I. Henry, L. D. Marks and R. P. Van Duyne, *Phys. Chem. Chem. Phys.*, 2013, **15**, 4110–4129.
15 N. Yamamoto, S. Ohtani and F. J. García De Abajo, *Nano Lett.*, 2011, **11**, 91–95.
16 K. Ikeda, K. Takahashi, T. Masuda and K. Uosaki, *Angew. Chem., Int. Ed.*, 2011, **50**, 1280–1284.
17 C. Du, C. Du, Y. You, C. He, J. Luo and D. Shi, *Plasmonics*, 2012, **7**, 475–478.
18 S. Mubeen, S. Zhang, N. Kim, S. Lee, S. Krämer, H. Xu and M. Moskovits, *Nano Lett.*, 2012, **12**, 2088–2094.
19 C. Ciracì, R. T. Hill, J. J. Mock, Y. Urzhumov, A. I. Fernández-Domínguez, S. A. Maier, J. B. Pendry, A. Chilkoti and D. R. Smith, *Science*, 2012, **337**, 1072–1074.
20 M. Sarkar, M. Besbes, J. Moreau, J. F. Bryche, A. Olivéro, G. Barbillon, A. L. Coutrot, B. Bartenlian and M. Canva, *ACS Photonics*, 2015, **2**, 237–245.
21 R. T. Hill, J. J. Mock, Y. Urzhumov, D. S. Sebba, S. J. Oldenburg, S.-Y. Chen, A. A. Lazarides, A. Chilkoti and D. R. Smith, *Nano Lett.*, 2010, **10**, 4150–4154.
22 M. Hu, A. Ghoshal, M. Marquez and P. G. Kik, *J. Phys. Chem. C*, 2010, **114**, 7509–7514.
23 J. J. Mock, R. T. Hill, A. Degiron, S. Zauscher, A. Chilkoti and D. R. Smith, *Nano Lett.*, 2008, **8**, 2245–2252.
24 C. Lumdee, B. Yun and P. G. Kik, *J. Phys. Chem. C*, 2013, **117**, 19127–19133.
25 J. J. Mock, R. T. Hill, Y. J. Tsai, A. Chilkoti and D. R. Smith, *Nano Lett.*, 2012, **12**, 1757–1764.
26 J. Mertens, A. L. Eiden, D. O. Sigle, F. Huang, A. Lombardo, Z. Sun, R. S. Sundaram, A. Colli, C. Tserkezis, J. Aizpurua, S. Milana, A. C. Ferrari and J. J. Baumberg, *Nano Lett.*, 2013, **13**, 5033–5038.
27 P. Nordlander and E. Prodan, *Nano Lett.*, 2004, **4**, 2209–2213.
28 X. Wang, M. Li, L. Meng, K. Lin, J. Feng, T. Huang, Z. Yang and B. Ren, *ACS Nano*, 2014, **8**, 528–536.
29 Z. Li, Y. Xiao, Y. Gong, Z. Wang, Y. Kang, S. Zu, P. M. Ajayan, P. Nordlander and Z. Fang, *ACS Nano*, 2015, **9**, 10158–10164.
30 G. M. Akselrod, T. Ming, C. Argyropoulos, T. B. Hoang, Y. Lin, X. Ling, D. R. Smith, J. Kong and M. H. Mikkelsen, *Nano Lett.*, 2015, **15**, 3578–3584.
31 Z. Li, G. Ezhilarasu, I. Chatzakis, R. Dhall, C. C. Chen and S. B. Cronin, *Nano Lett.*, 2015, **15**, 3977–3982.
32 H. Wang, T. Liu, Y. Huang, Y. Fang, R. Liu, S. Wang, W. Wen and M. Sun, *Sci. Rep.*, 2014, **4**, 7087.
33 W. H. Park, S. H. Ahn and Z. H. Kim, *ChemPhysChem*, 2008, **9**, 2491–2494.
34 M. Rycenga, X. Xia, C. H. Moran, F. Zhou, D. Qin, Z. Y. Li and Y. Xia, *Angew. Chem., Int. Ed.*, 2011, **50**, 5473–5477.
35 K. Kim, J. Y. Choi and K. S. Shin, *J. Phys. Chem. C*, 2013, **117**, 11421–11427.
36 H. A. Atwater and A. Polman, *Nat. Mater.*, 2010, **9**, 205–213.
37 J. D. Driskell, R. J. Lipert and M. D. Porter, *J. Phys. Chem. B*, 2006, **110**, 17444–17451.

38 L. Rodríguez-Lorenzo, R. A. Álvarez-Puebla, I. Pastoriza-Santos, S. Mazzucco, O. Stéphan, M. Kociak, L. M. Liz-Marzán and F. J. G. De Abajo, *J. Am. Chem. Soc.*, 2009, **131**, 4616–4618.
39 Y. Fang and Y. Huang, *Appl. Phys. Lett.*, 2013, 102.
40 J. Hao, T. Liu, Y. Huang, G. Chen, A. Liu, S. Wang and W. Wen, *J. Phys. Chem. C*, 2015, **119**, 19376–19381.
41 C. Lumdee, B. Yun and P. G. Kik, *Nanoscale*, 2015, **7**, 4250–4255.
42 Y. Chu and K. B. Crozier, *Opt. Lett.*, 2009, **34**, 244–246.
43 M. Shioi, H. Jans, K. Lodewijks, P. Van Dorpe, L. Lagae and T. Kawamura, *Appl. Phys. Lett.*, 2014, 104.
44 F. Zhou, Y. Liu and W. Cai, *Opt. Lett.*, 2014, **39**, 1302–1305.
45 H. Liu, Z. Yang, L. Meng, Y. Sun, J. Wang, L. Yang, J. Liu and Z. Tian, *J. Am. Chem. Soc.*, 2014, **136**, 5332–5341.
46 A. Taflove and S. C. Hagness, *Computational electrodynamics: the finite-difference time-domain method*, Artech House, Boston, 3rd edn., 2005.
47 P. B. Johnson and R. W. Christy, *Phys. Rev. B: Solid State*, 1972, **6**, 4370–4379.
48 E. D. Palik and G. Ghosh, *Handbook of optical constants of solids III*, Academic Press, San Diego, 1998.
49 W. L. Barnes, A. Dereux and T. W. Ebbesen, *Nature*, 2003, **424**, 824–830.
50 C. Sönnichsen, T. Franzl, T. Wilk, G. Von Plessen, J. Feldmann, O. Wilson and P. Mulvaney, *Phys. Rev. Lett.*, 2002, **88**, 774021–774024.
51 K. Lodewijks, J. Ryken, W. Van Roy, G. Borghs, L. Lagae and P. Van Dorpe, *Plasmonics*, 2013, **8**, 1379–1385.